Journal of the Australian Ceramic Society (2025) 61:937–951
https://doi.org/10.1007/s41779-024-01113-8

RESEARCH

Spark plasma sintering of B_4C-TiB_2 composite: Effect of combustion synthesized nanoparticle on sinterability and mechanical properties

Ozan Coban[1,2] · **Mehmet Bugdayci**[3,4] · **Salih Çagri Ozer**[5] · **Serkan Baslayici**[4] · **Servet Turan**[5] · **M. Ercan Acma**[2]

Received: 29 January 2024 / Revised: 29 July 2024 / Accepted: 20 October 2024 / Published online: 3 January 2025

Abstract

This study investigated the effects of fine particles with high surface area synthesized by Self-propagating High-Temperature Synthesis (SHS) on the SPS process and the properties of the resulting products. Correlations were established between particle size, SHS product addition, sinterability, and mechanical properties. The products were characterized by measuring shrinkage percentages, relative density, microhardness, elastic modulus, and fracture toughness, which were further correlated with SEM–EDS results. The results revealed that SHS nanoparticles significantly increased fracture toughness, especially with additions above 60%, by reducing average particle size, increasing powder porosity, and adding composite powder. The product exhibited high relative density (99.03%), elastic modulus (464 GPa), and fracture toughness (4.65 $MPa.m^{1/2}$) when SPS was used on B_4C-TiB_2 powders containing 80% SHS product at a low temperature of 1550 °C. By adding 80% SHS product, hardness increased by 62% (19.5 GPa) and fracture toughness by 24%, even at low sintering temperatures, thus reducing energy consumption.

Keywords Self-propagating high temperature synthesis · SHS · Spark plasma sintering · Boron carbide · Titanium diboride · Fracture toughness

Introduction

Boron Carbide (B_4C) and Titanium Diboride (TiB_2) are promising advanced ceramics due to their unique physical, mechanical, and thermal properties. By virtue of these properties, they have wide usage areas in critical technology fields such as the aerospace and defence industries. Some important application areas for B_4C can be summarized as armour applications, abrasive powders and hard coatings, neutron absorbers in the nuclear industry, and high-temperature semiconductors in the electronics industry [1–9]. TiB_2 is similarly used in abrasive and cutting tools thanks to its high hardness and wear resistance; it has high toughness, thermal shock resistance, corrosion resistance, and good thermal and electrical conductivity [10–14]. In order to provide the combination of these superior properties exhibited by both materials, the fabrication of a composite structure is significant. The low toughness of B_4C is its most important limiting property. In addition, strong covalent bonding, low thermal conductivity, low plasticity, and the oxide layer formed on the surface significantly reduce the sintering ability. Few studies have demonstrated that fracture toughness and sintering ability can be increased in combination with TiB_2 [15–19].

Spark Plasma Sintering (SPS) is a valuable method for producing high-performance advanced ceramics, offering several advantages over traditional sintering techniques. The most promising features of SPS reported in the literature are its high sintering rate and low sintering temperature, which result in a fine-grained structure, high pressure that eliminates porosity and forms strong bonds between particles, low contamination risk due to its operation under vacuum

---

✉ Mehmet Bugdayci
mehmet.bugdayci@yalova.edu.tr

[1] Gedik Vocational School, Machinery and Metal Technologies Dep., Istanbul Gedik University, Istanbul, Turkey

[2] Metallurgical and Materials Engineering Dep., Istanbul Technical University, Istanbul, Turkey

[3] Chemical Engineering Dep., Yalova University, 77200 Yalova, Turkey

[4] Vocational School, Construction Technology Dep., Istanbul Medipol University, İstanbul, Turkey

[5] Department of Materials Science and Engineering, Eskisehir Technical University, 26555 Eskisehir, Turkey

or argon atmosphere, and low dwelling duration, leading to homogenous distributions [20–23]. Researchers suggest that SPS is a promising method for fabricating B_4C-TiB_2 composites with improved properties. This is achieved through the mechanisms of binding effect, grain growth inhibition, and crack deflection, thanks to the compressive residual stress on the grain boundaries caused by the thermal expansion difference [24–30]. Recent studies have demonstrated the potential of SPS in producing B_4C-TiB_2 composites with improved properties, including a B_4C-TiB_2 composite with a fracture toughness of 4.36 MPa.$m^{1/2}$ at 1950 °C sintering temperature and 50 MPa pressure by Liu et al. [24], a B_4C-TiB_2 composite with a fracture toughness of 3.7 MPa.$m^{1/2}$ at 1900 °C sintering temperature and 50 MPa pressure by Rubink et al. [27], and a fracture toughness of 4.5 MPa.$m^{1/2}$ by Huang et al. [30], who applied pulsed electric current SPS at 2000 °C and 60 MPa. The mechanical properties of B_4C-TiB_2 composite are directly related to the composition. Researches have been carried out on different compositions. In Huang et al.'s study [30], it was revealed that the optimum results in terms of hardness and fracture toughness was obtained as the TiB_2 content was selected as 40% by volume (54% by weight). For this reason, this study focused on 50% (by wt.) TiB_2 content.

Particle size of powder is an important factor in the sintering process and must be optimized for desired properties. Niu et al. [31] studied the impact of TiB_2 particle size on the mechanical properties of B_4C-TiB_2 composites produced through pressureless sintering at 2100 °C. The addition of TiB_2 particles with a size of 500 nm up to 20% by weight increased the fracture toughness from 3.7 MPa.$m^{1/2}$ to 4.46 MPa.$m^{1/2}$. The highest fracture toughness value of 5.47 MPa.$m^{1/2}$ was obtained with the addition of TiB_2 particles with a sizes of 500 nm and 50 nm at 20% and 10% by weight, respectively. Liu et al. [32] investigated the effect of B_4C particle size on the production of B_4C-TiB_2 composites by hot pressing at 2000 °C and 35 MPa pressure. The highest fracture toughness value of 5.23 MPa.$m^{1/2}$ was achieved with a particle size of 7 µm. Zhao et al. [33] determined that the optimum B_4C particle size for TiB_2-B_4C composites was 0.5 µm, resulting in the highest fracture toughness value of 4.6 MPa.$m^{1/2}$. Guo et al. [34] established a relationship between ball milling time, TiB_2 particle size, and mechanical properties of B_4C-TiB_2 composites sintered by hot pressing. The fracture toughness increased from 4.80 MPa.$m^{1/2}$ to 7.69 MPa.$m^{1/2}$ due to the reduction of TiB_2 particle size from 5.94 µm to 1.96 µm after a 12-h ball milling.

The size of particles in the production of B_4C-TiB_2 is important in determining its sinterability and mechanical properties. One method that is commonly used is self-propagating high temperature synthesis (SHS), which produces fine powders with a high surface area due to their porosity. Turan et al. [35] conducted a study to examine the effects of adding SHS-produced nanoparticles with a size of 200 nm to sinter powder with a size of 6 µm on the relative density and hardness of TiB_2 produced by SPS at 1600 °C and 50 MPa. The study found that the addition of 50% SHS product to the sinter powder resulted in a significant increase in both relative density and hardness values in TiB_2 that produced by SPS. Specifically, the relative density increased from 76.75% to 96.34%, and the hardness value increased from 5.41 GPa to 21.48 GPa. However, there are only a few studies on the production of advanced ceramics using SPS from powders synthesized by SHS. Licheri et al. [36] used SHS to produce ZrB_2-SiC and HfB_2-SiC ultra-high temperature ceramics, which were fully consolidated by SPS at 1800 °C and 20 MPa. The authors reported that the combination of the SHS and SPS processes significantly reduced the sintering temperature and times. They compared the relative density values of SHS-SPS and reactive SPS composites and found that full densification could be achieved at 1800 °C with 20 min dwelling time by SHS-SPS, while it required 1900 °C with 30 min dwelling time by reactive SPS. At 1600 °C, the obtained relative density values were 97.5% and 82.5% for SHS-SPS and reactive SPS, respectively. Liu et al. [37] used SHS to produce TiB_2-Si composite powders, which were then consolidated by SPS at temperatures ranging from 1250–1350 °C and 50 MPa. Musa et al. [38] investigated the production of $TiC_{0.7}/TiB_2$ composites using SHS powders via SPS, and they found that near-fully densified composites could be produced at a temperature of 1400 °C and pressure of 20 MPa.

Other advanced ceramic composites that have been produced using the combination of SHS and SPS processes include HfB_2-$HfSi_2$ [39], HfB_2-SiC [40], NbC-NbB_2 [41], TaB_2-SiC [42], and ZrB_2-ZrC [43]. However, this study focuses on B_4C-TiB_2 production and aims to investigate the impact of adding self-propagating high-temperature synthesized powder on the effectiveness of the spark plasma sintering process and the mechanical properties of the resulting product. Additionally, the study aims to establish correlations between the average particle size of the sintering powder and the relative density, microhardness, and fracture toughness of B_4C-TiB_2 produced by SPS, which constitutes a novel contribution.

Materials and methods

During the first stage of experimental studies, the sintering capabilities of B_4C-TiB_2 composites, which were obtained by ball milling of commercially produced powders, were investigated. Micronized (20 µm) B_4C commercial powder, produced by carbothermal reduction (with an average particle size of 24 µm, as reported by Li et al. [44]) and fine-grained (200 nm) TiB_2 commercial powders produced by magnesiothermic reduction were subjected to a planetary ball milling process, which caused the formation of B_4C-TiB_2 composite powder that has particle size lower than that of B_4C and higher than that of TiB_2. The chemical compositions of the commercial powders used in experimental studies are given in Table 1. Ball milling processes were carried out for 1 h and 6 h, and sinter powders (sinter powder means the raw powder mixture utilized in the SPS process) with average particle sizes of 10 µm and 5 µm were obtained, respectively. B_4C grinding balls were used to prevent contamination during the ball milling processes. The powder-to-ball ratio was optimized to 1:7 by weight, and 1/4 of the balls having a diameter of 3 mm and 3/4 having a diameter of 10 mm. The ball milling process was applied at a frequency of 35 Hz.

The B_4C-TiB_2 powder, with an average particle size of 5 µm, was prepared by grinding commercial powders. The chemical composition of SHS product is given in Table 1. Additionally, the synthesis conditions of these powders can be found in the studies by Coban et al. [45–47]. The powders were mixed at varying ratios (20–80% by wt. for SHS powder) using a turbula mixer. The sintering process was carried out at 1550 °C. Furthermore, the B_4C-TiB_2 powders produced by ball milling for 6 h with an average particle size of 5 µm were also subjected to sintering at 2150 °C. The study investigated the effect of the average particle size and ball milling duration, the influence of SHS product addition, and the effect of sintering temperature. The production process flowchart of B_4C-TiB_2 composite by the Spark Plasma Sintering method is illustrated in Fig. 1.

The Spark Plasma Sintering (SPS) furnace (HP 25D, FCT GmbH, Germany) was used to consolidate the powders shown in Fig. 1. The powders were loaded into a 20 mm diameter graphite mould that was covered with graphite and pre-pressed manually under a pressure of 10 MPa. The mould and powders were then placed in the SPS furnace. The sintering process was carried out for 10 min, applying a pressure of 40 MPa and heating at a rate of 100 °C/min. The temperature was measured using an optical pyrometer, and the sintering was performed in a vacuum atmosphere of 10^{-2} bar at the temperatures specified in Fig. 1.

Microstructural characterization, phase analysis, crack length examination, microhardness testing and Vickers indentation fracture toughness determination of sintered samples were carried out by using an optical microscope (Leica Dmi8) and microhardness device (Emcotest DuraScan 70 G5). Previously, metallographic sample preparation was performed using a cBN abrasive grinder and a 3 µm

Table 1 Chemical compositions of commercial and SHS synthesized powders used in experimental studies (%, wt.)

	B	Ti	C	Ca	Fe	Si	Mg	O, F, Cl
B_4C (Commercial)	80,0	-	18,1	0,3	1,0	0,5	-	0,10
TiB_2 (Commercial)	31,0	68,0	-	-	-	0,14	0,2	0,66
B_4C-TiB_2 (SHS)	55,5	34,6	9,0	-	-	-	0,45	0,45

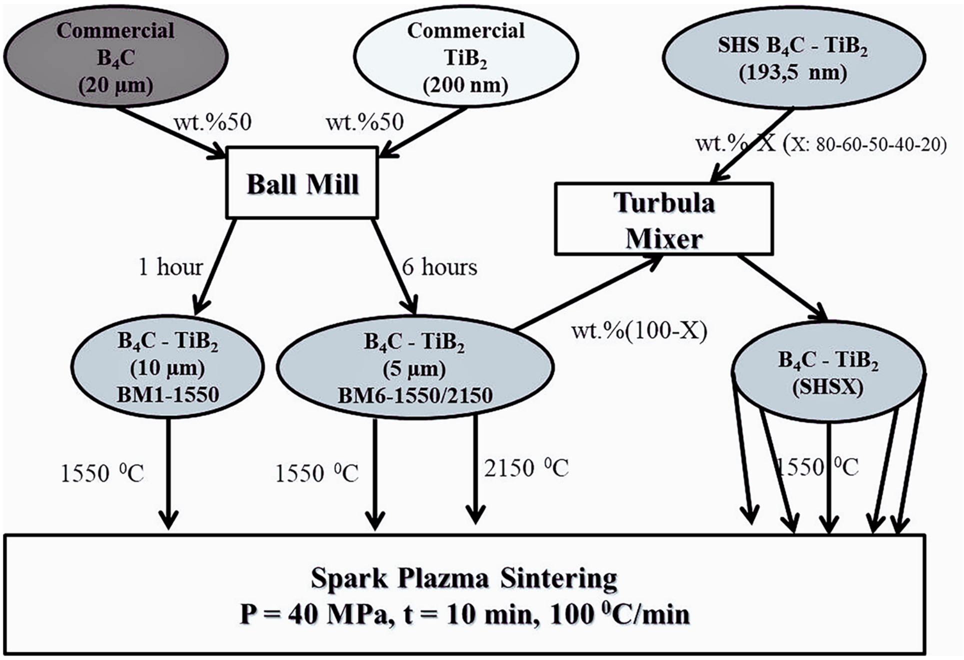

Fig. 1 Flowchart of experimental study

diamond suspension. 5 kgf (HV5) and 10 kgf (HV10) test methods were applied in the microhardness test. Microstructural examination, elemental mapping and analysis processes were carried out with an EDS-equipped scanning electron microscope (SEM–EDS) (JEOL JSM-6060 LV 15 kV). Agilent Technologies Nanoindenter G200 was used to determine the modulus of elasticity values needed for fracture toughness examination. Relative densities were determined with the principle of Archimedes. Six different models were applied in Fracture Toughness (K_{IC}) calculations, and values were determined for all samples according to each model.

Results and discussions

Characterization results of powders produced by SHS used in the SPS process are given in Fig. 2. As shown in Fig. 2a, SHS products have an average particle size of about 200 nm. The XRD result in Fig. 2b indicates that the main peaks are TiB_2 and B_4C. The results of the SEM–EDS analysis performed at the points shown in Fig. 2c are provided in Fig. 2d, which reveal that at point 1, besides TiB_2, B_4C is also present, indicating that the SHS product is in a composite structure.

After subjecting commercial powders to planetary ball milling for 6 h, a sinter powder with an average particle size of approximately 5 µm was produced. Figure 3a and b show SEM images of this powder. SEM images of sinter powder containing 50% SHS product and having an average particle size of 2.6 µm are given in Fig. 3c and d. The SEM images reveal that the structure includes coarse (about 10 µm) B_4C powders, as well as much finer-grained B_4C powders and TiB_2 nanoparticles. Comparing Figs. 3a and c, it can be seen that the SHS product additive significantly reduced the average particle size of the sintering powder. SEM–EDS analysis and elemental mapping were performed on commercial sintering powder, and the results are given in Fig. 3e. The presence of oxygen was detected at the surface boundary line of the large-grained B_4C phases, and the higher concentration of boron in these areas suggests that the B_2O_3 phase is present on the surface. Additionally, it is observed that the fine particles on the surface also contain some oxide and consist to a significant extent of the TiB_2 phase. The high boron content in certain areas of the fine-grained phases indicates the presence of fine-grained B_4C phases in addition to TiB_2. It was observed that the B_4C particles were partially transformed into finer particles due to the ball milling effect.

The dimensional changes of the powder given by the motion of the piston (relative piston travel, mm), which applies the pressure during sintering, and the sintering regime (pyrometer, °C) during the SPS processes are given in Fig. 4a-c. As shown in Fig. 4a, an increase in dimension was observed due to the expansion of the graphite mould. At a certain temperature, expressed as the shrinkage start temperature (Ts), a negative dimensional change occurs, as expected. This marked the start of sintering and shrinkage,

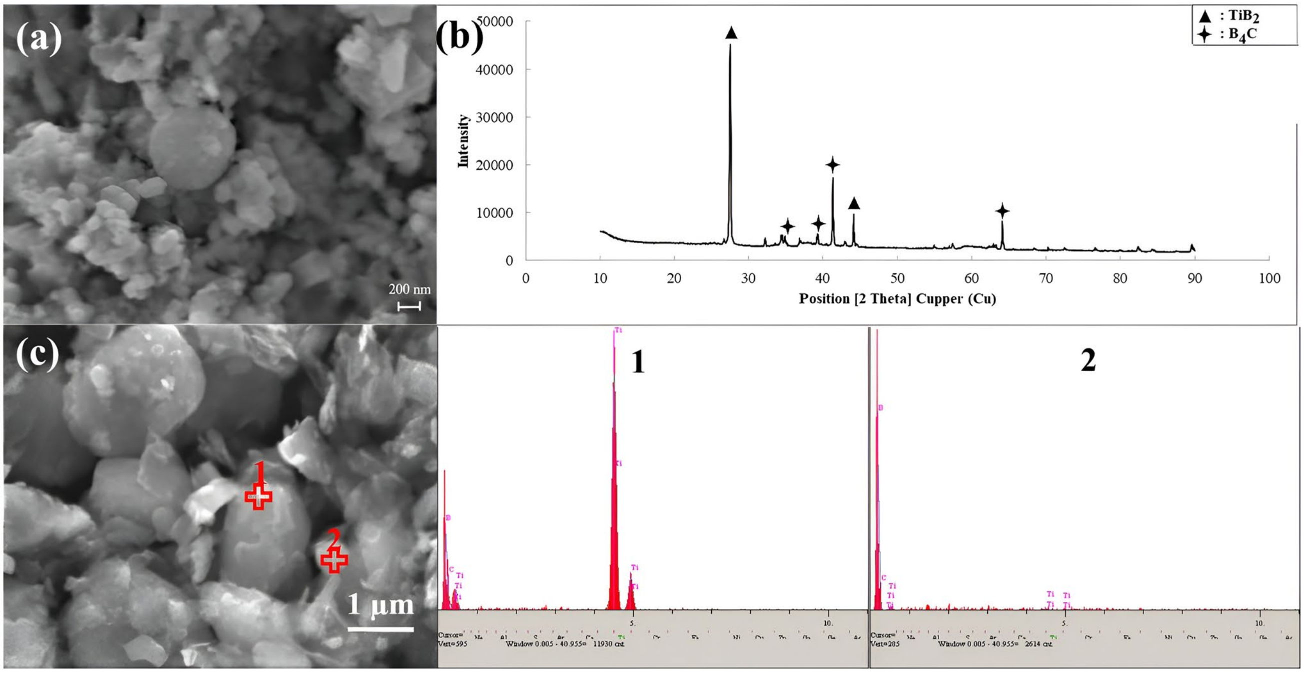

Fig. 2 Characterization results of SHS powders utilized in SPS (**a**) SEM image, (**b**) XRD analysis result, (**c**) EDS analysis points, (**d**) EDS analysis results

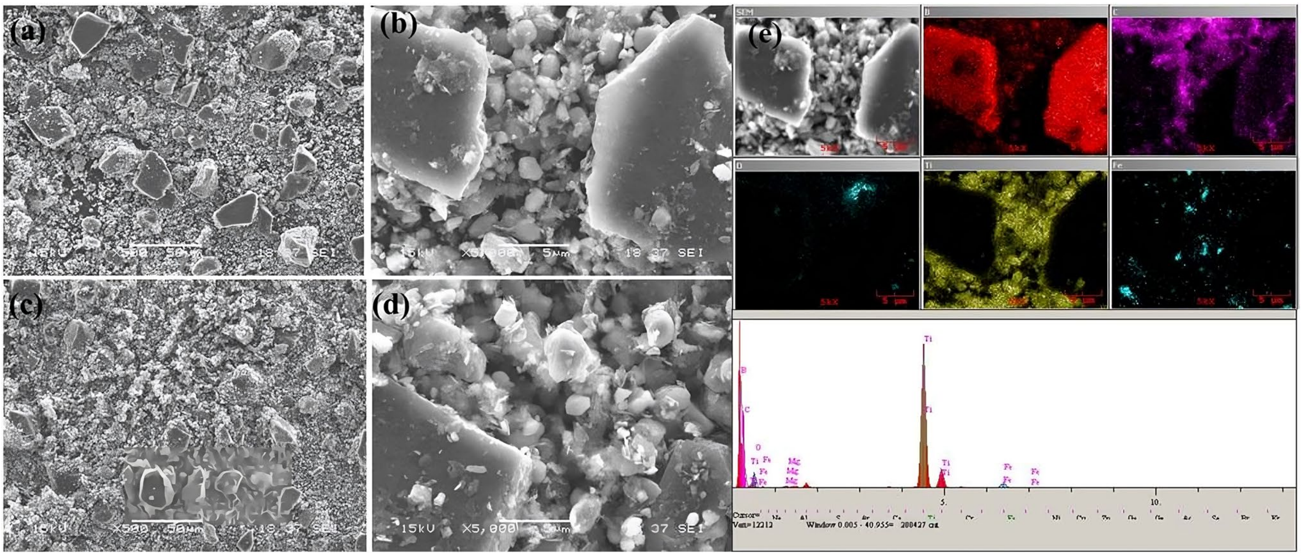

Fig. 3 SEM images of powders utilized in SPS (**a**), (**b**) 6-h ball milled commercial powder, (**c**), (**d**) 50% SHS product added powder; (**e**) SEM–EDS mapping results of commercial powder

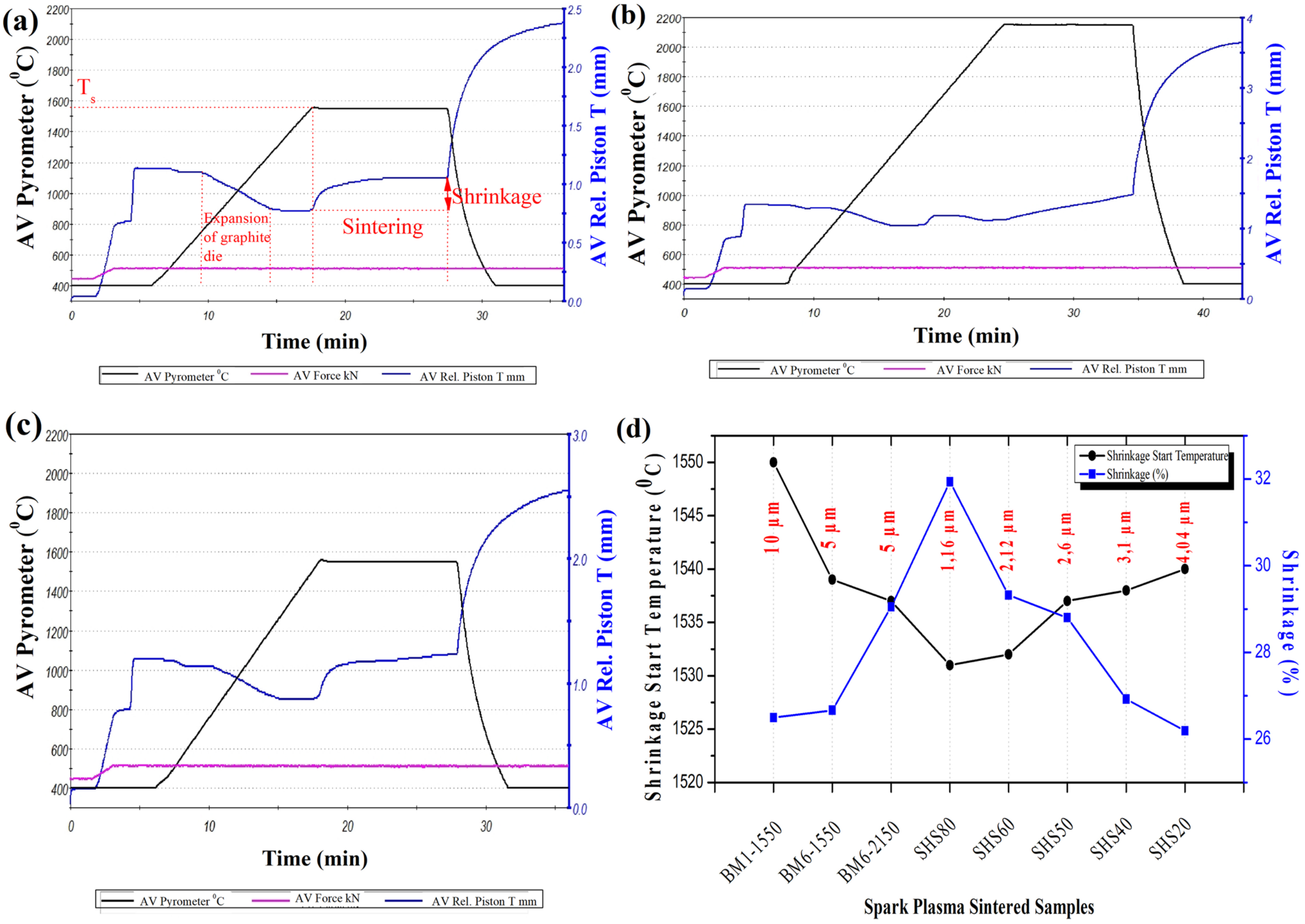

Fig. 4 Temperature, force and relative piston position change over time during SPS of (**a**) BM6-1550, (**b**) BM6-2150, (**c**) SHS50; and (**d**) shrinkage starting temperatures and shrinkage percentages of samples

which proceeded at rates dependent on the sinterability of the powder. At the temperature of 2150 °C during the process shown in Fig. 4b, a decrease in size was observed at approximately 1800 °C. This was attributed to the melting of iron from the commercial powder, which was visible as solidified ejections. The shrinkage percentages and Ts values for each sample, along with the average particle sizes of powders, are provided in Fig. 4d. The results indicated that the powder containing 80% SHS product exhibited the highest shrinkage percentage when sintered at 1550 °C (SHS80). This suggests that the shrinkage process began at lower temperatures compared to other experiments, possibly due to the addition of SHS product in the powder mixture.

In general, an inverse relationship was observed between the average particle size of the sinter powder and both the shrinkage starting temperature and the shrinkage percentage. As the ball milling time or the SHS product addition increased, leading to a decrease in the average particle size of the sinter powder, the shrinkage starting temperature decreased and the shrinkage percentage increased.

SEM images of the sintered B_4C-TiB_2 samples are given in Fig. 5a-c. It can be seen that the powders with an average particle size of 5 µm, which were obtained by ball milling for 6 h and did not contain SHS product, could not achieve sufficient consolidation during the sintering process. It was found that sinterability slightly improved as the temperature was increased to 2150 °C. The SEM image of the product obtained by sintering powder with an average particle size of 2.6 µm at 1550 °C, with 50% SHS product addition, is given in Fig. 5c. This image reveals that the addition of SHS product significantly enhanced sinterability. The SEM–EDS mapping result of the SHS50 sample given in Fig. 5d. It indicates that the sintered product consists of both coarse and fine B_4C grains, as well as fine TiB_2 grains. The coarse B_4C grains observed in the material are a result of the commercial powder used, while the fine B_4C grains are attributed to the combination of the SHS product and the effects of ball milling. As a result, TiB_2 grains on the surface of coarse B_4C grains provided good densification by providing a binding effect. By the virtue of the reduction of the particle size, more B_4C-TiB_2 interfaces were created, which improved the sinterability.

The effect of the SHS product addition and sintering temperature on the grain size of the B_4C phases in the product was investigated using an optical microscope. Phase analysis colour images of SHS50, BM6-1550, BM6-2150 and BM1-1550 samples are given in Fig. 6. Thus, it can be observed that the B_4C grain size is influenced by the presence of the SHS product and the ball milling process. Specifically, the SHS50 sample has the finest B_4C grain size, whereas the grain size increases in samples without SHS product. Additionally, the BM6-2150 sample, sintered at a high temperature, has the coarsest B_4C grains. These observations are depicted in Fig. 6, with Fig. 6a showing the SHS50 sample, Fig. 6b showing the BM6-1550 sample, and Fig. 6c showing the BM6-2150 sample. The amount of fine B_4C phases decreased significantly as the ball milling duration was reduced to 1 h as seen in Fig. 6d.

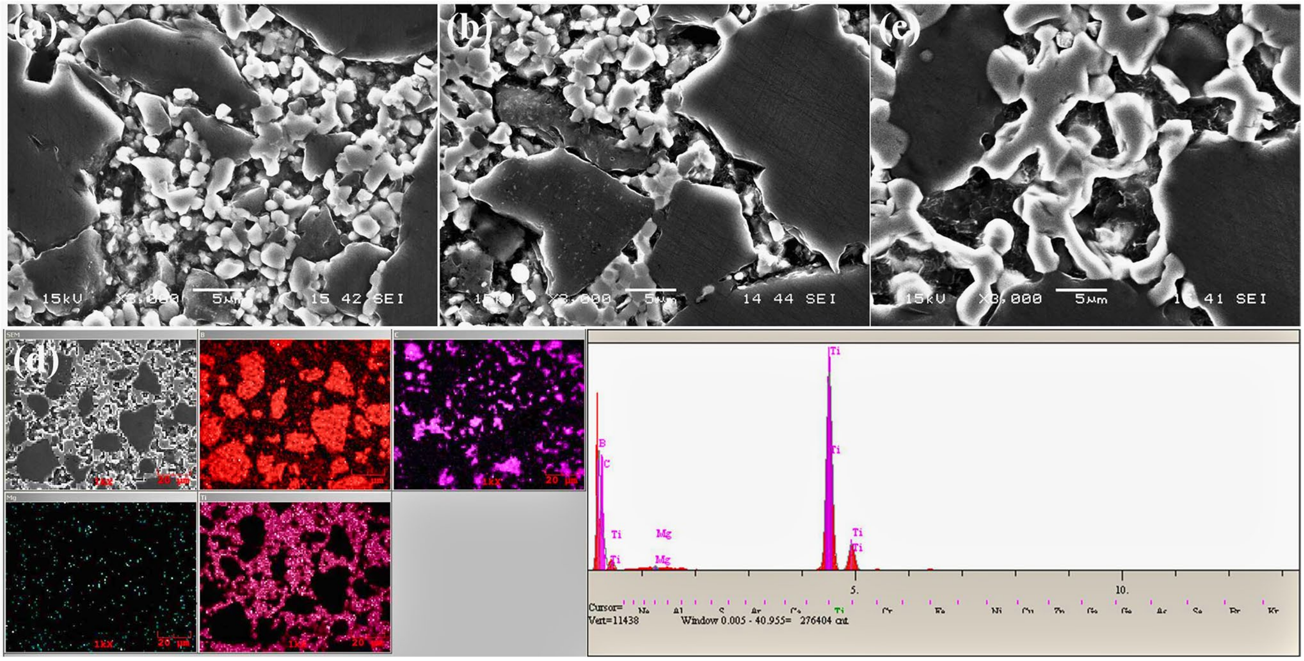

Fig. 5 SEM images of sintered samples (**a**) BM6-1550, (**b**) BM6-2150, (**c**) SHS50; and (**d**) SEM–EDS mapping results of SHS50 sintered sample

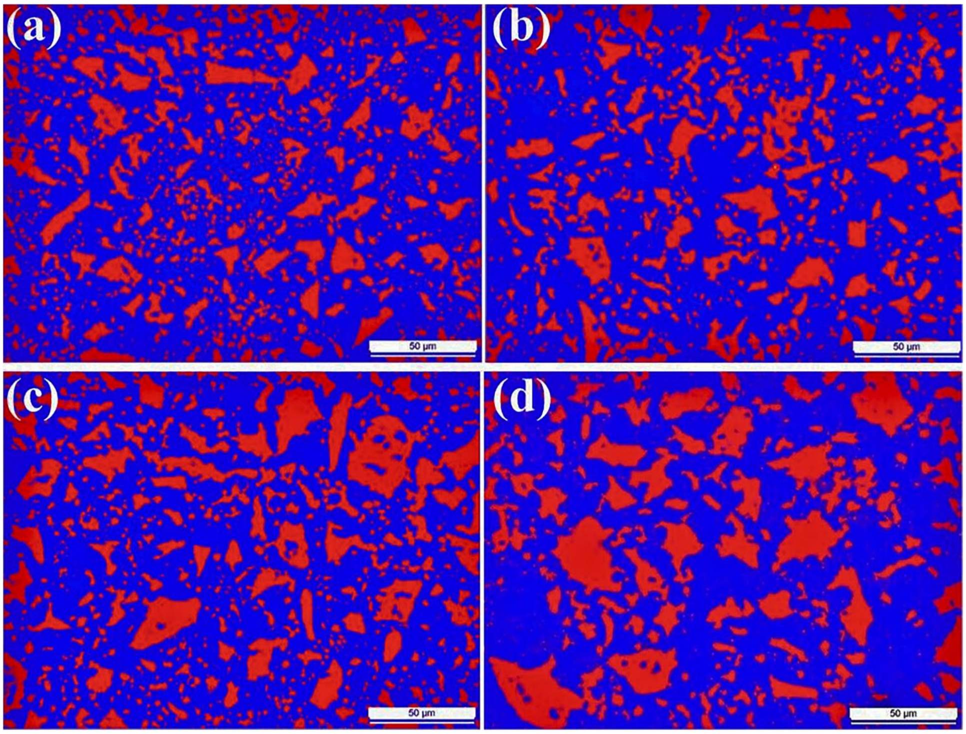

Fig. 6 Optical microscopy B_4C phase analysis results for (**a**) SHS50 (**b**) BM6-1550, (**c**) BM6-2150, (**d**) BM1-1550

The relative densities of the sintered B_4C-TiB_2 composite samples are given comparatively in Fig. 7a. The sample BM1-1550, which was sintered from composite powder with a particle size of around 10 µm using 1-h ball milling, had a relative density of 90.42%. However, when the ball milling time was increased to 6 h and the particle size was decreased to approximately 5 µm, the BM6-1550 sample exhibited a higher relative density of 92.44%. The highest relative density value of 99.19% was obtained as a result of sintering this powder at 2150 °C. A similar relative density could be achieved at lower temperatures (1550 °C) by adding 80% SHS product. Figure 7b shows the relationship between the SHS product addition ratio in the sintered powder and the relative density of the sintered product. Accordingly, it has been determined that the addition of SHS product over 20% provided a significant increase in relative densities. The relative density exceeded the average trend when the SHS product addition surpassed 40%.

The hardness test results on the SPS samples are given in Fig. 8a, along with the average particle sizes of the sintering powders. It is observed that the hardness values are closely

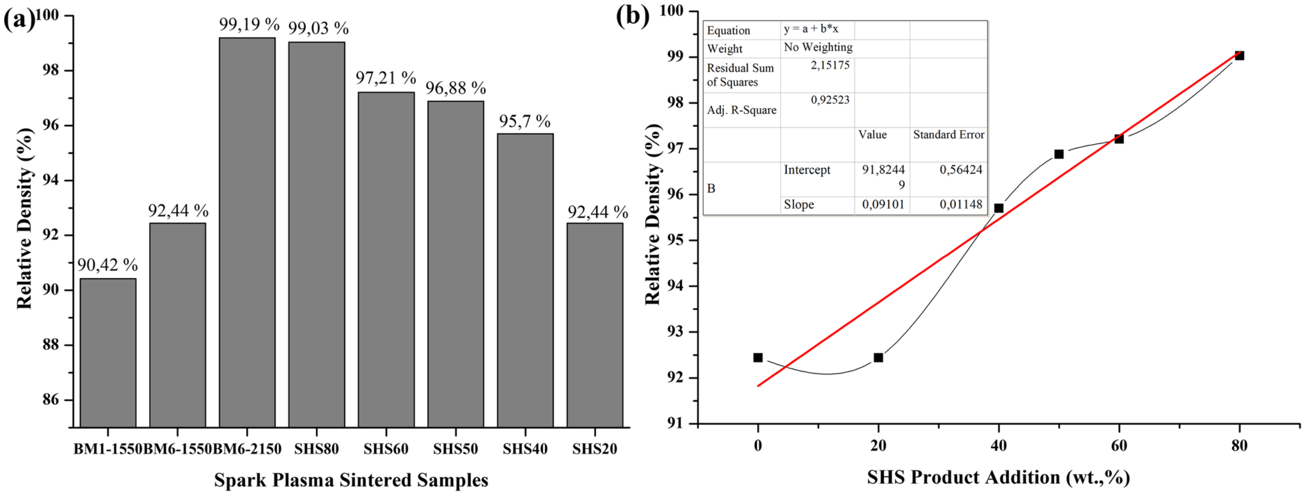

Equation	y = a + b*x		
Weight	No Weighting		
Residual Sum of Squares	2,15175		
Adj. R-Square	0,92523		
		Value	Standard Error
B	Intercept	91,82449	0,56424
	Slope	0,09101	0,01148

Fig. 7 Results for relative density determination (**a**) relative density values of sintered samples, (**b**) effect of SHS product addition on the relative density of B_4C-TiB_2

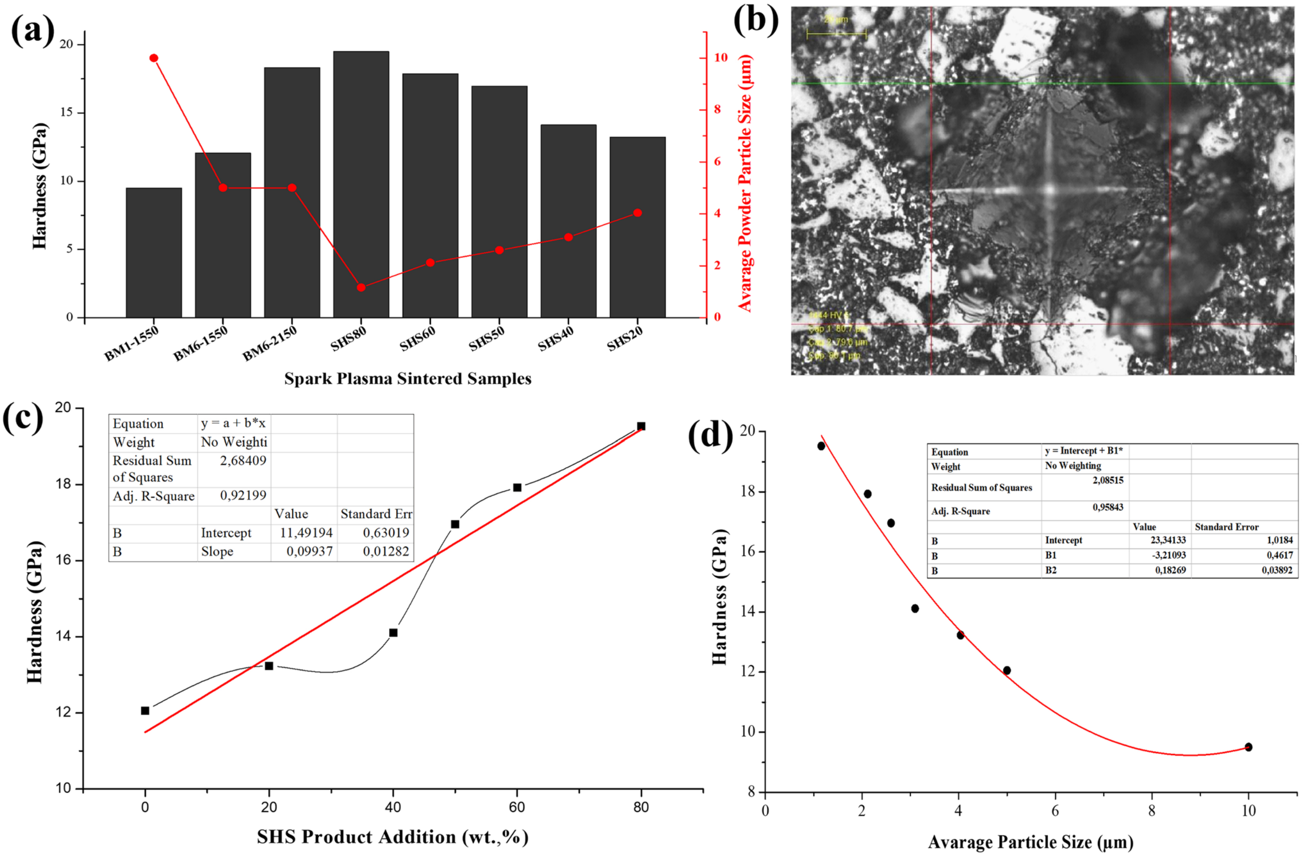

Fig. 8 Microhardness test results of B_4C-TiB_2 composite (**a**) microhardness of sintered samples, (**b**) microhardness measurement, and the relationship between microhardness and (**c**) SHS product addition, (**d**) average particle size of sintering powder

aligned with the relative density results, as expected. Comparing the hardness of the BM6-2150 and SHS80 samples, which both have a relative density of over 99%, reveals that a higher hardness value can be achieved with the addition of 80% SHS product, even at a much lower sintering temperature. When compared with the hardness of BM6-1550 (12.05 GPa), which was sintered at the same temperature and did not contain any SHS product, it has been determined that the addition of 80% SHS product increased the hardness by 62%. Figure 8c illustrates the relationship between the mass percent of the SHS product in the sintered powder and the hardness values of the sintered product. Accordingly, it has been determined that the SHS product addition of over 40% provided a significant increase in hardness values. When SHS product addition exceeded 50%, the hardness values were above the average trend. Figure 8d shows the relationship between the average particle size of the sinter powder and the hardness, indicating that the powder particle size has a significant effect on the hardness. The polynomial correlation given in Eq. 1, where HV_{10} represents hardness in GPa and d_{avg} represents average particle size in μm, was established between the average particle size and hardness for the B_4C-TiB_2 composite containing equal amounts of boron carbide and titanium diboride by mass.

$$HV_{10} = 2381.94 - 327.75 \times d_{avg} + 18.65 \times {d_{avg}}^2 \qquad (1)$$

Calculation of the stress intensity factor (K_{IC}) value to determine the fracture toughness has been suggested as another method other than the impact test for advanced ceramics. The Vickers indentation method is the most commonly used technique for determining the fracture toughness of brittle ceramic materials. In this method, the type of crack resulting from the Vickers hardness test (Palmqvist crack, radial-median crack, or a combination of both) is identified, and calculations are performed using mathematical models based on crack length, indentation diameter, HV hardness value, applied load, and modulus of elasticity [48–58]. Table 2 presents the fracture toughness calculation models proposed by researchers based on the crack mode. The images in Fig. 8b and Fig. 9a-d show the formation of a radial-median cracks in the samples.

Table 2 Models for fracture toughness calculation

Model / Eq. Number	Equation	Models	References
Radial-Median Crack			
2	$K_{IC} = 0{,}0309x\frac{F}{C^{3/2}}x(\frac{E}{HV})^{2/5}$	Nihara, Morena, Hasselman	[59, 60]
3	$K_{IC} = 0{,}016x\frac{F}{C^{3/2}}x(\frac{E}{HV})^{1/2}$	Anstis, Chantikul, Lawn, Marschall	[61–64]
4	$K_{IC} = 0{,}010x\frac{F}{C^{3/2}}x(\frac{E}{HV})^{2/3}$	Laugier	[65]
5	$K_{IC} = 0{,}024x\frac{F}{C^{3/2}}x(\frac{E}{HV})^{1/2}$	Casselas	[66]
6	$K_{IC} = 0{,}0752x\frac{F}{C^{3/2}}$	Evans and Charles	[58, 66, 67]
Any Crack Type			
7	$K_{IC} = 0{,}024x(\frac{E}{HV})^{2/5}xHVxa^{1/2}x(\frac{C}{a})^{-1{,}56}$	Lankford	[58, 68]

K_{IC}: Fracture Toughness ($MPa.m^{1/2} \times 10^6$)

F: Force applied in Vickers test (N)

C: Average distance from indentation center to crack tip (m)

E: Modulus of Elasticity (GPa)

HV: Vickers Hardness (GPa)

a: Mean value of Vickers indentation radius (m)

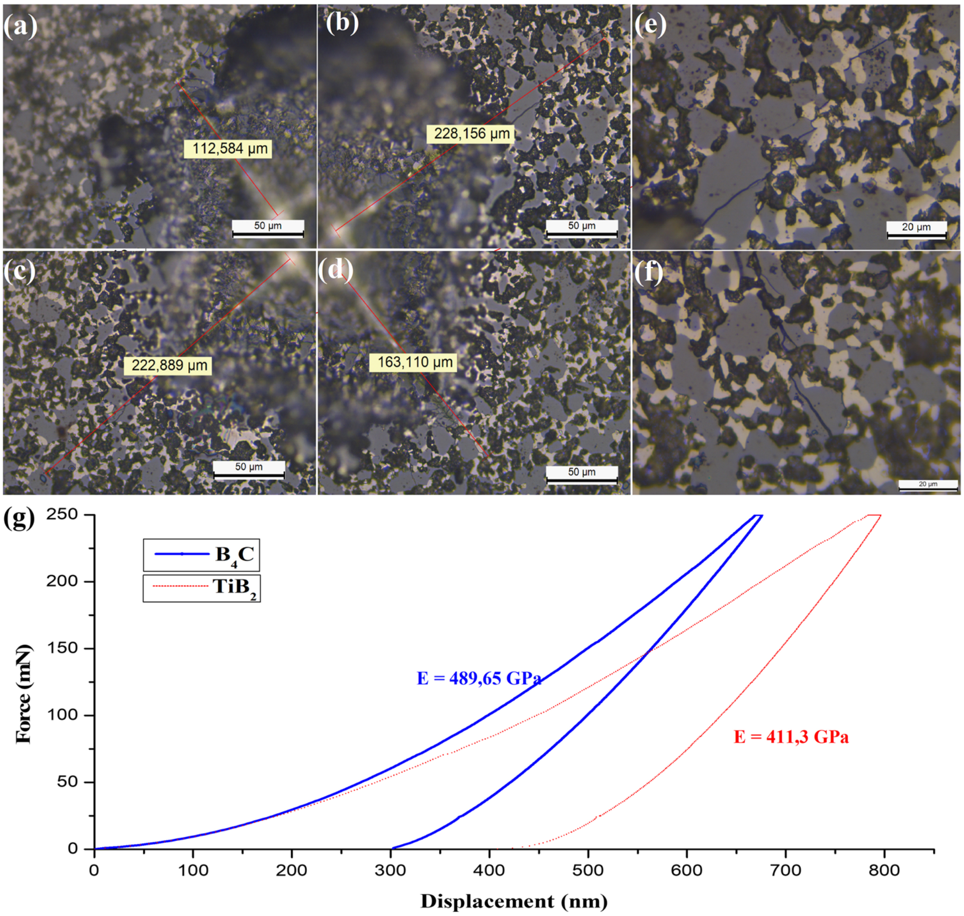

Fig. 9 (**a**)-(**d**) Crack length measurements, (**e**), (**f**) microstructures of crack propagation (**g**) average displacement changes over force values obtained by nano indentation tests

Fracture toughness was calculated by measuring crack length using the Vickers indentation method. In the calculations, six different models listed in Table 2 were used, and the results were compared. Figure 9a-d shows crack length measurements for the BM6-2150 sample as an example. In addition to calculating fracture toughness values, the crack propagation mechanism during Vickers indentation was also investigated. As shown in Fig. 9e-f, the crack generally progressed over coarse-grained B_4C phases. When it encountered TiB_2 phases or fine-grained B_4C phases, it moved towards the coalescence boundary and continued over TiB_2 phases at a minimal level. This toughening mechanism, called crack deflection, is caused by the difference in the thermal expansion coefficients of the phases ($8.1\times10^{-6}/^0C$ for TiB_2 and $4.5\times10^{-6}/^0C$ for B_4C) [31, 69, 70]. Crack branching mechanism was also observed, as seen in Fig. 9f. The nanoindentation method, also known as depth-sensing indentation, is commonly used to determine the modulus of elasticity of multiphase advanced ceramic materials. This method allows for the determination of the modulus of elasticity of each individual phase separately since the mechanical properties of multi-phase advanced ceramic materials are orientation-dependent. The general modulus of elasticity of the material is then determined over the volume fractions of the phases using the law of mixtures. In this study, the elasticity modules were calculated by measuring the depth change at nanoscale under 250 mN force by increasing the speed of 10 mN/s by using a cube corner Berkovich diamond tip on the B_4C and TiB_2 phases. Force–displacement diagrams obtained over the average values of 10 different measurements are given in Fig. 9g for both phases. Modulus of elasticity values were calculated by the Oliver-Pharr method [71]. The modulus of elasticity of B_4C-TiB_2 was determined as 464.29 GPa, based on the law of mixtures. Calculation of fracture toughness according to Nihara, Morena, Hasselman model given in Eq. 2 (Model/Eq. Number 2 in Table 2) is given in Eq. 8.

$$K_{IC} = 0.0309x\frac{F}{C^{\frac{3}{2}}}x\left(\frac{E}{HV}\right)^{\frac{2}{5}} = 0.0309x\frac{98}{(181.68x10^{-6})^{\frac{3}{2}}}x\left(\frac{469.29}{18.326}\right)^{\frac{2}{5}} = 4.5245\ \text{MPa.m}^{1/2} \tag{8}$$

Figure 10a shows fracture toughness values obtained by the Vickers indentation method for six different models, excluding the Evans and Charles model, which calculates independently of the elasticity modulus. These values were determined using elasticity modulus values obtained from nanoindentation tests and are compared for four samples. The average values for each model are represented by a star symbol. Accordingly, the highest fracture toughness value was obtained in the SHS80 sample. When evaluated using the Nihara, Morena, and Hasselman model, it can be seen that adding 80% SHS product increased the fracture toughness by 24%. Increasing the sintering temperature from 1550 °C to 2150 °C, rather than using SHS product, resulted in a 20% increase in fracture toughness. Figure 10b shows the relationship between the mass percent of the SHS product in the sinter powder and the fracture toughness values of the sintered product. Accordingly, it was determined that adding more than 60% SHS product significantly increased fracture toughness. When the SHS product addition exceeded 70%, the fracture toughness values were notably above the average trend.

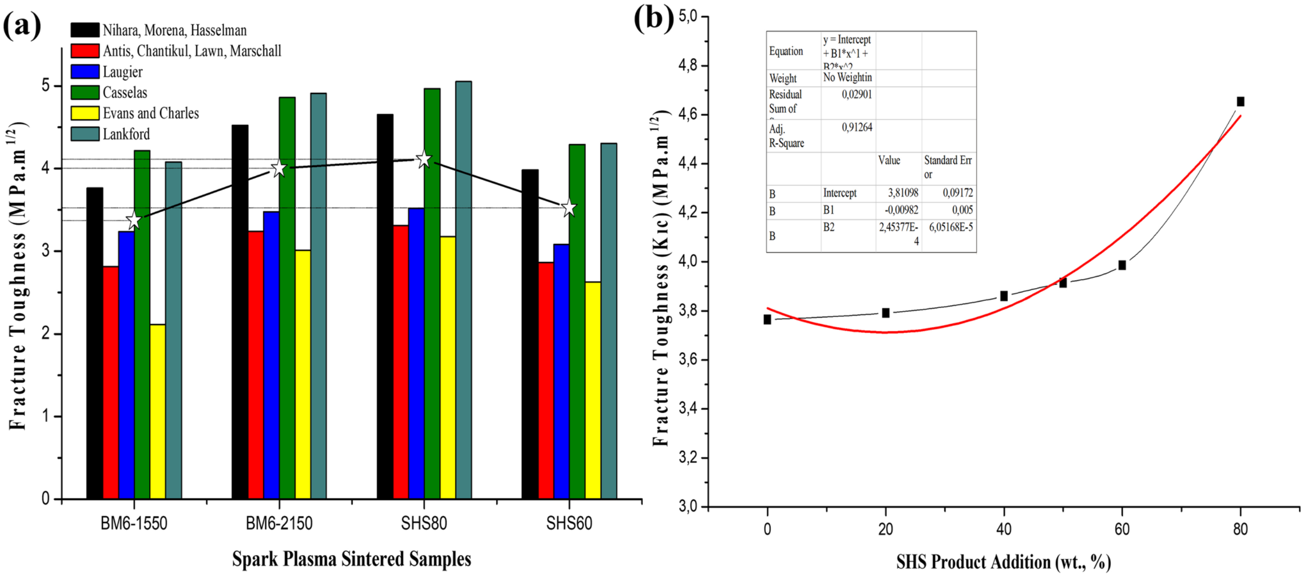

Fig. 10 (**a**) Fracture toughness values of sintered samples for 6 different models, (**b**) effect of SHS product addition on fracture toughness of B_4C-TiB_2

Table 3 Comparison of B_4C-TiB_2 product properties and process parameters reported in recent years

Sintering Method	Product / Temperature (^{0}C) / Pressure (MPa)	Avarage Particle Sizes (μ) (B_4C / TiB_2)	Relative Density (%)	Hardness (GPa)	Fracture Toughness, Kıc (MPa. $m^{1/2}$)	Ref. (year)
Pressureless Sintering	*B_4C-30TiB_2 / 2100	3 / 7 + 0,5 + 0,05	98,6	30,19	5,47	Niu et al. [31] (2021)
	*B_4C-20TiB_2 / 2175	1 / 0,08 (TiO_2)	98	31,79	3,51	Heydari et al. [74] (2015)
	B_4C-30TiB_2 / 2150	1,33 / -	98,5	22,99	3,4	Baharvandi et al. [72] (2008)
Reactive Hot Pressing	B_4C–20TiB_2 / 1950 / 30 MPa	2,5 / 1,96	99,2	32,51	7,69	Guo et al. [34] (2023)
	B_4C–24TiB_2 / 2100 / 60 MPa	-	97,2	31,99	3,9	F. Sahin et al. [75] (2009)
	B_4C–30TiB_2 + SiC / 1950 / 60 MPa	3 / 3 (TiC)	99,4	32,99	6,5	Zhang et al. [76] (2017)
Spark Plasma Sintering	B_4C–35TiB_2 / 1950 / 50 MPa	2,10 / 3,72	96,71	28,81	4,36	Yingying Liu et al. [24] (2020)
	B_4C–30TiB_2 / 1800–2000 / 50 MPa	2,10 / 3,72	98,47	29,81	3,7	Yingying Liu et al. [25] (2020)
	B_4C–30TiB_2 / 1900 / 50 MPa	~ 1 / ~ 1	100	29,99	8	Husarova et al. [26] (2018)
	B_4C–20TiB_2 / 1900 / 50 MPa	2,1 / 2,6	99,4	34,99	3,7	Rubink et al. [27] (2021)
	*B_4C–15TiB_2 / 2250 / 50 MPa	- / < 0,1	94,5	25,50	4,38	Moradkhani et al. [77] (2016)
	*33B_4C–33TiB_2-33SiC / 1800 / 75 MPa	0,45 / 3	100	33,00	4,05	Rodríguez-Rojaz et al. [29] (2023)
	***B_4C-50TiB_2 / 1550 / 40 MPa**	**5 / 0,19**	**99,03**	**19,51**	**4,65**	**Present study**
Pulsed Electric Current SPS	*B_4C–54TiB_2 / 2000 / 60 MPa	0,5 / 3	100	30,50	4,5	Huang et al. [30] (2011)

*: studies investigating the effect of particle size and/or using submicron powders

The best properties for the B_4C-50% TiB_2 composite were achieved through the SPS process by sintering composite powders with an average particle size of 1.16 µm and 80% SHS product addition at 1550 °C. The relative density, hardness, and fracture toughness values were 99.03%, 1991 HV, and 4.65 MPa.$m^{1/2}$, respectively. Table 3 and Fig. 11 (for SPS) present a comparison of the values obtained in this study with the results reported in recent studies. Stoichiometric ratios are provided as percentages by weight. The results indicate that, despite the very low sintering temperature used in this study, good consolidation and relative density were achieved, and the fracture toughness was higher than that reported in similar studies in the literature. The relatively low hardness values can be attributed to the high TiB_2 content and low sintering temperature. For example, in Baharvandi et al.'s study [72], the hardness of the composite containing 30% TiB_2 decreased to approximately 2000 HV. The study indicates that as the TiB_2 content exceeded 15%, the hardness decreased. Another study conducted by Srivatsan et al. [73] revealed that as TiB_2 content increased from 5 to 15%, hardness increased from 35.72 GPa to 38.61 GPa; however, as it increased up to 25%, the increase in hardness became minor, reaching 39.55 GPa. Additionally, increasing the sintering temperature resulted an increase in hardness. The study by Rodríguez-Rojaz et al. [29], presented in Table 3, reported that at a sintering temperature of 1600 °C using SPS, a hardness of 2650 HV was achieved, which increased to 3367 HV at 1800 °C. It should be noted that the higher sintering pressure and the presence of SiC as a third phase should also be considered.

Conclusion

The production of a B_4C-TiB_2 ceramic composites with excellent mechanical properties is crucial for technological advancements. the Spark Plasma Sintering (SPS) is considered the most appropriate method for manufacturing such materials. Improving the sintering capability in the SPS process remains a challenging area of research, particularly

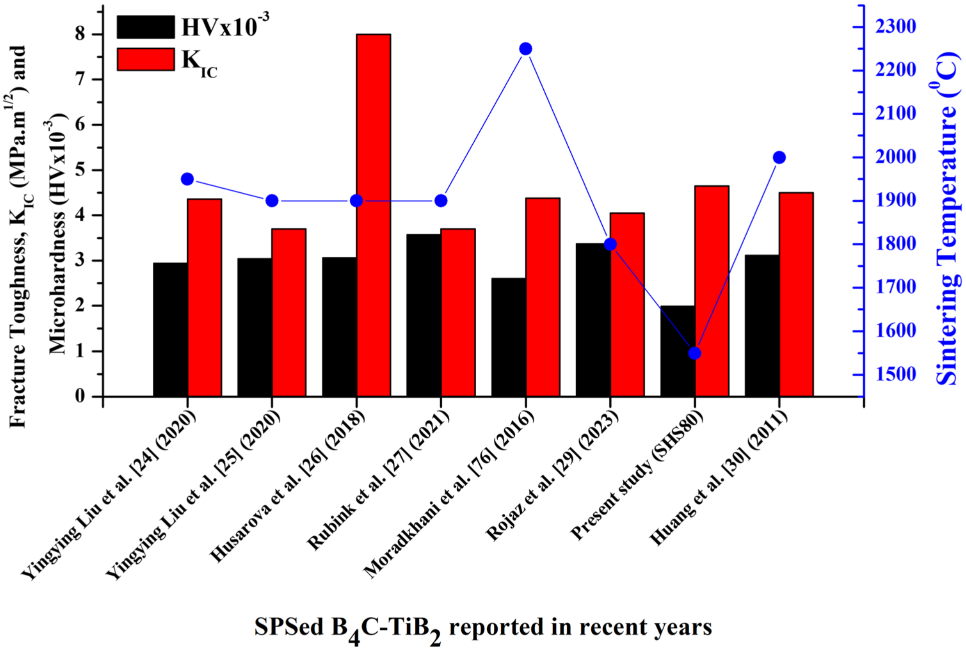

Fig. 11 Comparison of SPSed B_4C-TiB_2 product properties and sintering temperatures reported in recent years

for producing B_4C-TiB_2 ceramic composites. In this study, we investigated the effect of adding B_4C-TiB_2 powder, with a particle size of 193.5 nm produced by Self-Propagating High-Temperature Synthesis (SHS), to commercial powders on sinterability. We examined how this addition affected the relative density, microhardness, modulus of elasticity, and fracture toughness of the sintered product. Additionally, we established the relationship between the average particle size of the sintering raw materials and their mechanical properties. The following results were obtained:

1- In the SPS processes to produce B_4C-TiB_2 composites, a low relative density (90.42%) was achieved in the sintering of commercial powders with an average particle size of 10 µm obtained by a 1-h ball mill at 1550 °C sintering temperature. When the ball milling duration was increased to 6 h, the relative density slightly improved (92.44%) for powders with a particle size of 5 µm, also sintered at 1550 °C. A high consolidation and relative density value (99.19%) was achieved by increasing the sintering temperature to 2150 °C. However, it was found that nearly the same consolidation and relative density could be achieved by adding 80% by weight of SHS product instead of significantly increasing the temperature.

2- Microhardness test results showed that the hardness of the sample sintered at 1550 °C from the composite powder containing 80% SHS product was higher than that of the sample sintered at 2150 °C from the powder without SHS product. The addition of 80% SHS product resulted in a 62% increase in hardness, with a microhardness value of 1990 HV (19.5 GPa).

3- The modulus of elasticity of the phases forming the composite structure was determined using the nanoindentation method. The volumetric phase fraction was determined by optical microscope phase analysis and the modulus of elasticity ($E_{B4C\text{-}TiB2}$) of the composite was determined as 464 GPa. Fracture toughness was determined using the Vickers indentation method and analyzed with six different models. According to the results, the highest fracture toughness value was obtained in the sample produced by sintering the powder containing 80% SHS product, and this value was determined as 4.65 MPa.m$^{1/2}$ (according to the Nihara, Morena, Hasselman model). It was determined that 80% SHS product addition increased fracture toughness by 24%. The crack propagation mechanism was mostly intergranular, with deflection by fine TiB_2 particles. The toughening mechanisms were determined to be crack deflection and crack branching.

The results revealed that the addition of the fine particulate SHS product significantly lowered the SPS sintering temperatures and resulted in good mechanical properties. With an increase in the SHS product additive ratio, the improvements in properties exceeded the average trend, with increases of 40%, 50%, and 70% for relative density, hardness, and toughness, respectively. In other words, increasing the SHS product additive primarily contributed to improving relative density, significantly enhanced hardness values, and had a notable effect on fracture toughness at higher additive levels. Further studies could explore the effects of different sintering temperatures and the addition of a third metallic or ceramic phase to achieve even better mechanical properties.

Acknowledgements The authors would like to thank Istanbul Gedik University for their financial support to this study, which was carried out within the scope of the Scientific Research Project entitled "Production of Nano Composites of Boron Carbide-Titanium Diboride (B_4C-TiB_2) by Self-Propagating High Temperature Synthesis (SHS) and Spark Plasma Sintering" and numbered "GDK202207-46".

Data Availability No datasets were generated or analysed during the current study.

Declarations

Conflict of interest On behalf of all authors, the corresponding author states that there is no conflict of interest.

References

1. Koysuren, O., Koysuren, H.N.: Synthesis of B4C powder via the carbothermal reduction and photoreduction of Cr(VI) on B4C under visible light irradiation. J. Korean Ceram. Soc. (2023). https://doi.org/10.1007/s43207-023-00307-3
2. Li, X., Lei, M., Gao, S., Yan, S., Wang, X., Xing, P.: Effect of initial compositions on boron carbide synthesis and corresponding growth mechanism. Adv. Appl. Ceram. **118**(8), 442–450 (2019). https://doi.org/10.1080/17436753.2019.1664792
3. Crouch, I.G., Eu, B.: Ballistic testing methodologies. In: Crouch, I.G. (ed.) The science of armour materials, pp. 639–673. Elsevier, San Diego (2016)
4. Domnich, V., Reynaud, S., Haber, R.A., Chhowalla, M.: Boron Carbide: Structure, Properties and Stability Under Stress. J. Am. Ceram. Soc. **94**(11), 3605–3628 (2011). https://doi.org/10.1111/j.1551-2916.2011.04865.x
5. Savio, S.G., Sambasiva Rao, A., Rama Subba Reddy, P., Madhu, V.: Microstructure and ballistic performance of hot pressed & reaction bonded boron carbides against an armour piercing projectile. Adva. Appl. Ceram. **118**(5), 264–273 (2019). https://doi.org/10.1080/17436753.2018.1564416
6. Chen, S., Wang, D., Huang, J., Ren, Z.: Synthesis and characterization of boron carbide nanoparticles. Appl. Phys. A **79**, 1757–1759 (2004)
7. Wood, C.: Materials for thermoelectric energy conversion Rep. Prog. Phys. **51**(4), 459 (1988). https://doi.org/10.1088/0034-4885/51/4/001
8. Tucker M., Joseph H.C., Hou J., Li H., Lan Y.: A comprehensive review of boron carbide thermoelectic materials. Molecules (2020)
9. Sauerschnig, P., Watts, J.L., Vaney, J.B., Talbot, P.C., Alarco, J.A., Mackinnon, I.D.R., Mori, T.: Thermoelectric properties of phase pure boron carbide prepared by a solution-based method. Adv. Appl. Ceram. **119**(2), 97–106 (2020). https://doi.org/10.1080/17436753.2019.1705017
10. Tallon, C., Franks, G.V.: Exploring inexpensive processing routes to prepare dense TiB_2 components. Adv. Appl. Ceram. **115**(7), 403–410 (2016). https://doi.org/10.1080/17436753.2016.1172166
11. Mukhopadhyay, A., Raju, G.B., Basu, B., Suri, A.K.: Correlation between phase evolution, mechanical properties and instrumented indentation response of TiB_2-based ceramics. J. Eur. Ceram. Soc. **29**, 505–516 (2009)
12. Ricceri, R., Matteazzi, P.: A fast and low-cost room temperature process for TiB_2 formation by mechanosynthesis. Mater. Sci. Eng. A **379**, 341–346 (2004)
13. Górnya, G., Rączkaa, M., Stobierskia, L., Rożniatowskib, K., Rutkowskia, P.: Ceramic composite Ti3SiC2–TiB2-Microstructure and mechanical properties. Mater. Charact. **60**, 1168–1174 (2009)
14. Bilgi, E., Camurlu, H.E., Akgun, B., Topkaya, Y., Sevinc, N.: Formation of TiB_2 by volume combustion and mechanochemical process. Mater. Res. Bull. **43**, 873–881 (2008)
15. Madhav, R.K., Guo, J.J., Shinoda, Y., Fujita, T., Hirata, A., Singh, J.P., McCauley, J.W., Chen, M.W.: Enhanced mechanical properties of nanocrystalline boron carbide by nanoporosity and interface phases. Nat. Commun. (2012). https://doi.org/10.1038/ncomms2047
16. Heydari, M.S., Baharvandi, H.R.: Comparing the effects of different sintering methods for ceramics on the physical and mechanical properties of B_4C–TiB_2 nanocomposites. Int. J. Refract. Metals Hard Mater. **51**, 224–232 (2015)
17. Baharvandi, H.R., Hadian, A.M., Alizadeh, A.: Processing and Mechanical Properties of Boron Carbide-Titanium Diboride Ceramic Matrix Composites. Appl. Compos. Mater. **13**, 191–198 (2006). https://doi.org/10.1007/s10443-006-9012-0
18. Huang, S.G., Vanmeensel, K., Van der Biest, O., Vleugels, J.: In situ synthesis and densification of submicrometer-grained B_4C–TiB_2 composites by pulsed electric current sintering. J. Eur. Ceram. Soc. **31**, 637–644 (2011)
19. Xu, C., Cai, Y., Flodström, K., Li, Z., Esmaeilzadeh, S., Zhang, G.J.: Spark plasma sintering of B4C ceramics: the effects of milling medium and TiB2 addition. Int. J. Refract. Met. Hard. Mater. **30**, 139–144 (2012)
20. Tokita, M.: Progress of Spark Plasma Sintering (SPS) Method, Systems, Ceramics Applications and Industrialization. Ceramics **4**(2), 160–198 (2021). https://doi.org/10.3390/ceramics4020014
21. Stuer, M., Bowen, P., Zhao, Z.: Spark Plasma Sintering of Ceramics: From Modeling to Practice. Ceramics **3**(4), 476–493 (2020). https://doi.org/10.3390/ceramics3040039
22. Balaji, V.S., Kumaran, S.: Densification and microstructural studies of titanium–boron carbide (B4C) powder mixture during spark plasma sintering. Powder Technol. **264**, 536–540 (2014). https://doi.org/10.1016/j.powtec.2014.05.050
23. Savari, V., Balak, Z., Shahedifar, V.: Combined and alone addition effect of nano carbon black and SiC on the densification and fracture toughness of SPS-sintered ZrB_2. Diam. Relat. Mater. **128**, 109244 (2022). https://doi.org/10.1016/j.diamond.2022.109244
24. Liu, Y., Li, Z., Peng, Y., Huang, Y., Huang, Z., Zhang, D.: Effect of sintering temperature and TiB_2 content on the grain size of B_4C-TiB_2 composites. Mater. Today Commun. **23**, 100875 (2020). https://doi.org/10.1016/j.mtcomm.2019.100875
25. Liu, Y., Wu, X., Liu, M., Huang, Y., Huang, Z.: Microstructure and mechanical properties of B_4C–TiB_2–SiC composites fabricated by spark plasma sintering. Ceram. Int. **46**(3), 3793–3800 (2020). https://doi.org/10.1016/j.ceramint.2019.10.102
26. Husarova, I.O., Potapov, O.M., Solodkyi, I.V., Bogomol, I.I.: Production and Properties of B_4C–TiB_2 Composites with Isotropic Eutectic Microstructure. Powder Metall. Met. Ceram. **57**(3–4), 209–214 (2018). https://doi.org/10.1007/s11106-018-9970-4
27. Rubink, W., Ageh, V., Lide, H., Ley, N., Young, M., Casem, D., Faierson, E., Scharf, T.: Spark plasma sintering of B_4C and B_4C-TiB_2 composites: Deformation and failure mechanisms under quasistatic and dynamic loading. J. Eur. Ceram. Soc. **41**(6), 3321–3332 (2021). https://doi.org/10.1016/j.jeurceramsoc.2021.01.044
28. Kim, K.H., Chae, J.H., Park, J.S., Kim, D.K., Shim, K.B., Lee, B.H.: Sintering Behavior and Mechanical Property of B4C Ceramics Fabricated by Spark Plasma Sintering. J. Korean Ceram. Soc. **45**(1), 60 (2008). https://doi.org/10.4191/kcers.2008.45.1.060
29. Rodríguez-Rojas, F., Zamora, V., Guiberteau, F., Ortiz, A.L.: Solid-state spark plasma sintering of super wear resistant B4C–SiC–TiB2

triplex-particulate composites. Ceram. Int. **49**(3), 5532–5537 (2023). https://doi.org/10.1016/j.ceramint.2022.11.181

30. Huang, S., Vanmeensel, K., Malek, O., Van der Biest, O., Vleugels, J.: Microstructure and mechanical properties of pulsed electric current sintered B4C–TiB2 composites. Mater. Sci. Eng., A **528**(3), 1302–1309 (2011). https://doi.org/10.1016/j.msea.2010.10.022
31. Niu, H., Zhu, Y., You, N., Wang, Y., Cheng, H., Luo, D., Tang, M., Zhang, J.: Effects of TiB_2 Particles on the Microstructure Evolution and Mechanical Properties of B_4C/TiB_2 Ceramic Composite. Materials (Basel, Switzerland) **14**(18), 5227 (2021)
32. Liu, Z., Deng, X., Li, J., Sun, Y., Ran, S.: Effects of B4C particle size on the microstructures and mechanical properties of hot-pressed B4C–TiB2 composites. Ceram. Int. **44**(17), 21415–21420 (2018). https://doi.org/10.1016/j.ceramint.2018.08.200. (**ISSN 0272-8842**)
33. Zhao, J., Li, Q., Cao, W., Liu, Z., Deng, X., Ding, X., Ran, S.: Influences of B_4C content and particle size on the mechanical properties of hot pressed TiB_2–B_4C composites. J. Asian Ceram. Soc. **9**(3), 1239–1247 (2021). https://doi.org/10.1080/21870764.2021.1953759
34. Guo, W., He, Q., Wang, A., Tian, T., Liu, C., Hu, L., Wang, W., Wang, H., Fu, Z.: Effect of TiB_2 particles on microstructure and mechanical properties of B4C–TiB2 ceramics prepared by hot pressing. Ceram. Int. **49**(3), 4403–4411 (2023). https://doi.org/10.1016/j.ceramint.2022.09.327
35. Turan, A., Cinar, S.F., Goller, G., Yucel, O.: Spark Plasma Sintering Of Self-Propagating High-Temperature Synthesized TiB_2 Ceramics. Nano Studies **15–16**, 27–34 (2018)
36. Licheri, R., Orrù, R., Musa, C., Locci, A.M., Cao, G.: Spark Plasma Sintering of ZrB_2 – and HfB $_2$–Based Ultra HighTemperature Ceramics Prepared by SHS. Int. J. Self Propag. High Temp. Synth. **18**(1), 15–24 (2009)
37. Liu L., Aydinyan S., Minasyan T., Baronins J., Antonov M., Kharatyan S., Hussainova I., Spark Plasma Sintering of Combustion Synthesized TiB_2-Si Composite. Ceram. Modern Technol. **1** (2019). https://doi.org/10.29272/cmt.2018.0009
38. Musa, C., Locci, A.M., Licheri, R., Orrú, R., Cao, G., Vallauri, D., Deorsola, F.A., Tresso, E., Suffner, J., Hahn, H., Klimczyk, P., Jaworska, L.: Spark plasma sintering of self-propagating high-temperature synthesized $TiC_{0.7}/TiB_2$ powders and detailed characterization of dense product. Ceram. Int. **35**, 2587–2599 (2009)
39. Musa, C., Licheri, R., Orrù, R., Cao, G.: Synthesis, Sintering, and Oxidative Behavior of HfB2-HfSi2 Ceramics. Ind. Eng. Chem. Res. (2014). https://doi.org/10.1021/ie4032692
40. Licheri, R., Orrù, R., Musa, C., Locci, A.M., Cao, G.: Consolidation via Spark Plasma Sintering of HfB_2/SiC and HfB2/HfC/SiC Composite Powders obtained by Self-propagating Hightemperature Synthesis. J. Alloys Compd. **478**, 572–578 (2009)
41. Tsuchida, T., Kakuta, T.: Fabrication of SPS compacts from NbC–NbB2 powder mixtures synthesized by the MA–SHS in air process. J. Alloys Compd. **415**, 156–161 (2006)
42. Licheri, R., Orrù, R., Musa, C., Cao, G.: Synthesis, densification and characterization of TaB2-SiC composites. Ceram. Int. **36**, 937–941 (2010)
43. Tsuchida, T., Yamamoto, S.: Spark plasma sintering of ZrB_2–ZrC powder mixtures synthesized by MA-SHS in air. J. Mater. Sci. **42**, 772–778 (2007)
44. Li, X., Wang, S., Nie, D., Liu, K., Yan, S., Xing, P.: Effect and corresponding mechanism of NaCl additive on boron carbide powder synthesis via carbothermal reduction. Diam. Relat. Mater. **97**, 107458 (2019). https://doi.org/10.1016/j.diamond.2019.107458
45. Coban, O., Bugdayci, M., Acma, M.E.: Production of B_4C-TiB_2 composite powder by self-propagating high-temperature synthesis. J. Aust. Ceram. Soc. **58**, 777–791 (2022). https://doi.org/10.1007/s41779-022-00714-5
46. Coban, O., Bugdayci, M., Baslayici, S., Acma, M.E.: Combustion Synthesis of B_4C-TiB_2 Nanocomposite Powder: Effect of Mg Particle Size on SHS and Optimization of Acid Leaching Process. J. Superhard Mater. **45**(1), 20–30 (2023). https://doi.org/10.3103/S1063457623010033
47. Coban, O., Bugdayci, M., Baslayici, S., Acma, M.E.: Combustion Synthesis of B_4C–TiB_2 Composite Nanoparticle by Self-Propagating High-Temperature Synthesis (SHS) in B_2O_3–TiO_2–Mg–C System. In: Li, B., Ghosh, D., Olevsky, E.A., Lu, K., Dong, F., Li, J., Wang, R., Dupuy, A.D., Torresani, E., et al. (eds.) Advances in Powder and Ceramic Materials Science 2023. TMS 2023. The Minerals, Metals & Materials Series. Springer, Cham (2023). https://doi.org/10.1007/978-3-031-22622-9_16
48. Bonache, V., Salvadorv, B.D., Burguete, P., Martínez, E., Sapiña, F., Sánchez, E.: Synthesis and processing of nanocrystalline tungsten carbide: Towards cemented carbides with optimal mechanical properties. Int. J. Refract. Metals Hard Mater. **29**(1), 78–84 (2011). https://doi.org/10.1016/j.ijrmhm.2010.08.003
49. Fabijanić, T.A., Alar, E., Ćorić, D.: Influence of consolidation process and sintering temperature on microstructure and mechanical properties of near nano- and nano-structured WC-Co cemented carbides. Int. J. Refract Metal Hard Mater. **54**, 82–89 (2016). https://doi.org/10.1016/j.ijrmhm.2015.07.017
50. International Standard Organisation. ISO 28079:2009: Hardmetals-Palmqvist Toughness Test. Available online: https://www.iso.org/obp/ui/#iso:std:iso:28079:ed-1:v1:en. Accessed on 23 Nov 2022
51. Roebuck, B., Gee, M., Bennett, E.G., Morrell, R.: Mechanical tests for hardmetals. Measurement good practice guide No. 20, National physical laboratory, Teddington, UK. Crown Copyright, pp. 57–61 (1999) .
52. Antonov, M., Sergejev, F.: Comparative study on indentation fracture toughness measurements of cemented carbides. Proc. Estonian Acad. Sci. Eng. **12**(4), 388 (2006). https://doi.org/10.3176/eng.2006.4.07
53. Sheikh, S., M'Saoubi, R., Flasar, P., Schwind, M., Persson, T., Yang, J., Llanes, L.: Fracture toughness of cemented carbides: Testing method and microstructural effects. Int. J. Refract. Metal. Hard Mater. **49**, 153–160 (2015). https://doi.org/10.1016/j.ijrmhm.2014.08.018
54. Shetty, D.K., Wright, I.G., Mincer, P.N., Clauer, A.H.: Indentation fracture of WC-Co cermets. J. Mater. Sci. **20**(5), 1873–1882 (1985). https://doi.org/10.1007/bf00555296
55. Quinn, G.D., Bradt, R.C.: On the Vickers Indentation Fracture Toughness Test. J. Am. Ceram. Soc. **90**(3), 673–680 (2007). https://doi.org/10.1111/j.1551-2916.2006.01482.x
56. Cuadrado N., Casellas D., Llanes L., Gonzalez I., Caro J.: Effect of crystal anisotropy on the mechanical properties of WC embedded in WC-Co cemented carbides. Proceedings of the Euro International Powder Metallurgy Congress and Exhibition, Euro PM, **1**, 215-220 (2011).
57. Sebastiani, M., Johanns, K., Herbert, E., Pharr, G.: Measurement of fracture toughness by nanoindentation methods: Recent advances and future challenges. Curr. Opin. Solid State Mater. Sci. **19**(6), 324–333 (2015). https://doi.org/10.1016/j.cossms.2015.04.003
58. Şakar-Deliormanli, A., Güden, M.: Microhardness and fracture toughness of dental materials by indentation method. J. Biomed. Mater. Res. B Appl. Biomater. **76B**(2), 257–264 (2006). https://doi.org/10.1002/jbm.b.30371
59. Niihara, K.: A fracture mechanics analysis of indentation-induced Palmqvist crack in ceramics. J. Mater. Sci. Lett. **2**(5), 221–223 (1983). https://doi.org/10.1007/bf00725625
60. Niihara, K., Morena, R., Hasselman, D.P.H.: Evaluation of K1c of brittle solids by the indentation method with low crack-to-indent ratios. J. Mater. Sci. Lett. **1**, 13–16 (1982). https://doi.org/10.1007/BF00724706

61. Anstis, G., Chantikul, P., Lawn, B., Marshall, D.: A Critical Evaluation of Indentation Techniques for Measuring Fracture Toughness: I, Direct Crack Measurements. J. Am. Ceram. Soc. **64**(9), 533–538 (1981). https://doi.org/10.1111/j.1151-2916.1981.tb10320.x
62. Nastic, A., Merati, A., Bielawski, M., Bolduc, M., Fakolujo, O., Nganbe, M.: Instrumented and Vickers Indentation for the Characterization of Stiffness, Hardness and Toughness of Zirconia Toughened Al_2O_3 and SiC Armor. J. Mater. Sci. Technol. **31**(8), 773–783 (2015). https://doi.org/10.1016/j.jmst.2015.06.005
63. Moraes, M.C.C.D.S.E.B.D., Elias, C.D., Duailibi Filho, J., Oliveira, L.G.D.: Mechanical properties of alumina-zirconia composites for ceramic abutments. Mater. Res. **7**(4), 643–649 (2004). https://doi.org/10.1590/s1516-14392004000400021
64. Chantikul, P., Anstis, G.R., Lawn, B.R., Marshall, D.B.: A Critical Evaluation of Indentation Techniques for Measuring Fracture Toughness: II, Strength Method. J. Am. Ceram. Soc. **64**(9), 539–543 (1981). https://doi.org/10.1111/j.1151-2916.1981.tb10321.x
65. Laugier, M.T.: The elastic/plastic indentation of ceramics. J. Mater. Sci. Lett. **4**(12), 1539–1541 (1985). https://doi.org/10.1007/bf00721390
66. Aleksandrov, F.T., Ćorić, D., Šnajdar, M.M., Sakoman, M.: Vickers Indentation Fracture Toughness of Near-Nano and Nanostructured WC-Co Cemented Carbides. Metals **7**(4), 143 (2017). https://doi.org/10.3390/met7040143
67. Evans, A.G., Heuer, A.H., Porter, D.L.: The fracture toughness of ceramics. In: Taplin, D.M.R. (ed.) Proceedings of 4th International Conference on Fracture, pp. 529–556. New York: Plenum Press. (1977)
68. Ćorić, D., Ćurković, L., Majić Renjo, M.: Statistical Analysis of Vickers Indentation Fracture Toughness of Y-TZP Ceramics. Trans. FAMENA **41**(2), 1–16 (2017). https://doi.org/10.21278/tof.41201
69. Wu, Q.R., Wen, B.X.: Study on temperature dependence of thermal conductivity and linear expansion for SiC material. J. S. China Univ Technol. Nat. Sci. Ed. **24**, 11–15 (1996)
70. Einarsrud, M.A., Hagen, E., Pettersen, G., Grande, T.: Pressureless sintering of titanium diboride with nickel, nickel boride, and iron additives. J. Am. Ceram. Soc. **80**, 3013–3020 (2005)
71. Oliver, W.C., Pharr, G.M.: Measurement of hardness and elastic modulus by instrumented indentation: Advances in understanding and refinements to methodology. J. Mater. Res. **19**, 3–20 (2004)
72. Baharvandi, H., Hadian, A.: Pressureless Sintering of TiB_2-B_4C Ceramic Matrix Composite. J. Mater. Eng. Perform. **17**(6), 838–841 (2008). https://doi.org/10.1007/s11665-007-9182-4
73. Srivatsan, T.S., Guruprasad, G., Black, D., Radhakrishnan, R., Sudarshan, T.S.: Influence of TiB2 content on microstructure and hardness of TiB2–B4C composite. Powder Technol. **159**(3), 161–167 (2005). https://doi.org/10.1016/j.powtec.2005.08.003. (**ISSN 0032-5910**)
74. Saeedi, H.M., Baharvandi, H., Dolatkhah, K.: Effect of TiO_2 nanoparticles on the pressureless sintering of B_4C–TiB_2 nanocomposites. Int. J. Refract. Metal. Hard Mater. **51**, 6–13 (2015). https://doi.org/10.1016/j.ijrmhm.2015.01.014
75. Sahin, F.C., Yesilcubuk, S.A.: B_4C-TiB_2 Composites via Reactive Hot Pressing. High Temp. Mater. Process. (London) **28**(5), 277–284 (2009). https://doi.org/10.1515/htmp.2009.28.5.277
76. Zhang, X., Zhang, Z., Wang, W., Shan, J., Che, H., Mu, J., Wang, G.: Microstructure and mechanical properties of B_4 C-TiB_2 -SiC composites toughened by composite structural toughening phases. J. Am. Ceram. Soc. **100**(7), 3099–3107 (2017). https://doi.org/10.1111/jace.14815
77. Moradkhani, A., Baharvandi, H., Mohammadi Samani, M.M.: Mechanical properties and microstructure of B4C–NanoTiB_2–Fe/Ni composites under different sintering temperatures. Mater. Sci. Eng., A **665**, 141–153 (2016). https://doi.org/10.1016/j.msea.2016.04.034